

# Passivity-based Active Stabilization for DC Microgrid Applications

Jiaqi Yu, Jingrong Yu, Yue Wang, Yijia Cao, *Senior Member, IEEE*, Xiaonan Lu, *Member, IEEE*, and Dongbo Zhao, *Senior Member, IEEE*

**Abstract**—In this paper, an improved active stabilization strategy of the interface converters in microgrid applications is proposed on the basis of the passivity-based stability criterion (PBSC). As a critical part of AC and DC hybrid microgrids, the DC microgrid is taken as an example. In particular, a stabilization method with a proportional-integral (PI) controller and first-order high-pass filter (HPF) is proposed to meet the passivity requirements of the overall control diagram with respect to the output voltage. Meanwhile, an output current feedback control loop is introduced to ensure the output impedance passivity. Moreover, a small-signal model of the parallel interface converter system is established to comprehensively study the influence of control parameters on the passivity of the converters. Based on the active stabilization method proposed in this study, by manipulating the control diagram of each interface converter, the passivity and stability of the DC microgrids with variable configuration can be guaranteed. Therefore, a generic and simplified design approach is realized. A simulation model with three interface converters is implemented in MATLAB/Simulink, and the effectiveness of the proposed passivity-based active stabilization algorithm is verified by using this simulation model.

**Index Terms**—Microgrids, PBSC, small-signal model, stabilization.

## I. INTRODUCTION

AS a critical part of AC and DC hybrid microgrids, the DC microgrid is recently gaining more popularity with the wide use of DC power sources, energy storage, and loads with natural DC coupling [1]–[5]. Compared to their AC counterparts, DC microgrids feature the highlighted advantages of high efficiency, strong robustness and no need for harmonics and resynchronization, etc. [6], [7].

However, the degraded stability issues induced by interface converters should still be noted in DC microgrids. Typically,

Manuscript received October 8, 2016; revised March 20, 2017; accepted May 22, 2017. Date of publication March 30, 2018; date of current version December 25, 2017. This work was supported in part by the National Natural Science Foundation of China (Nos. 51137003, 61233008 and 51520105011), and in part by the Special Project of International Scientific and Technological Cooperation of China (No. 2015DFR70850).

J. Q. Yu and Y. J. Cao are with the College of Electrical and Information Engineering, Hunan University, Changsha 410082, China.

J. R. Yu (corresponding author e-mail: jingrong@mail.csu.edu.cn) and Y. Wang are with School of Information Science and Engineering, Central South University, Changsha 410083, China.

X. N. Lu is with the Energy Systems Division, Argonne National Laboratory, Lemont, IL 60439, USA.

D. B. Zhao is with Eaton Corporation, Eden Prairie, MN, USA.

DOI: 10.17775/CSEEJPES.2016.01390

each converter is designed as a stable module, while oscillations or destabilization may still take place in DC microgrids consisting of parallel converters. Impedance matching criterion is a commonly used approach for stability analysis. It was originally proposed by Middlebrook and used for studying the instability issues induced by the interacted input filters and load converters. The essence of these criteria is to evaluate the source and load impedance ratio by using Nyquist plots [8]. Although the Middlebrook criterion provides an effective approach for evaluating system stability, this method can lead to a conservative design. Therefore, several modified stability evaluation approaches implemented based on the Middlebrook criterion were proposed, including the gain margin phase margin (GMPM) criterion used for designing the input impedance of the load converter with a given source converter [9], the opposing argument criterion used for individual load converter design in the system with multiple parallel load converters [10], the energy source analysis consortium (ESAC) criterion focusing on total load design with given source converters [11], etc. These criteria provide a convenient technique to tackle the obstacles of the stability issues in DC microgrids. However, these criteria are used for the stability analysis with a fixed partition of source and load subsystems. If the role of the source and load changes, then the effectiveness of these criteria can be degraded [12], [13]. The passivity-based stability assessment method does not require the predetermined source and load partition. Hence, it is more flexible compared to the impedance criteria [13].

Two significant features of the passivity criterion include: 1) If a system is passive, it can be derived that this system is stable [14]; 2) The parallel or negative feedback connection of two passive systems derives a system that is still passive and thereby stable [15], [16]. As a result, once an individual converter in DC microgrids is designed as a passive module, the passivity and stability of the whole system can be ensured. Hence, the system-level design procedure can be simplified. Recently, the PBSC has been used in several studies on DC microgrids [15], [16]. The passivity-criterion is employed in [15], and the active damping method is used to ensure the passivity of the system's overall impedance, which thereby ensures the stability of the system. However, the structure of the DC system under study is only comprised of one converter with an LC filter and a constant power load (CPL), so various types of input perturbations should be considered when the PBSC is applied to the DC microgrids dominated by multiple

parallel converters. The system impedance angle in the passivity criterion is changed from  $[-90^\circ, 90^\circ]$  to  $[-30^\circ, 90^\circ]$  in [16] to increase the phase margin of the system and avoid the oscillations induced by insufficient damping. However, only the output admittance passivity is considered in this paper, which cannot ensure the stability of the bus voltage in DC microgrids. In an accurate small-signal model of DC microgrids, bus voltage stability is influenced by the perturbations of the converter output current, input voltage, and reference voltage. The existing PBSC only considers the perturbation in the output current, i.e. output impedance. Therefore, it cannot guarantee the stability of the bus voltage since the perturbations from the other two input channels are not fully evaluated. If the passivity of each converter under any perturbation is guaranteed, the DC microgrids with these parallel converters or feedback-connected converters are passive and thereby stable.

In this paper, a comprehensive PBSC with consideration of all input perturbations is introduced, which provides a generic criterion for each individual interface converter and guarantees the stable operation of the parallel-converter-dominated DC microgrids under different types of input perturbations. The control strategy is realized by adding an additional output current feedback control loop to the output side of the combined control diagram with a PI controller and a high-pass filter (HPF). The output impedance passivity is ensured by using the output current feedback control. Meanwhile, the passivity of the input voltage and reference voltage with respect to the output voltage is ensured by the combined control diagram with PI and HPF. The passivity and stability analyses are conducted by assessing the location of the closed-loop poles and Nyquist plots.

The following paper is organized as follows. The basic concepts of PBSC are introduced in Section II. The detailed mathematical model of the DC converter, as well as the passivity analysis, is established in Section III. The improved control strategy is proposed in Section IV to meet the PBSC requirements and ensure the stability of the DC microgrids. The simulation demonstration in MATLAB/Simulink is conducted in Section V to verify the effectiveness of the proposed active stabilization method. Finally, the major contributions of this paper are summarized in section VI.

## II. PASSIVITY-BASED STABILITY CRITERION

The passivity of the system can be defined by using the system state space functions. In order to interpret the nature of passivity-based criteria, the concept of energy injection is introduced [15]–[18]. In particular, the state space function of a linear system is described as follows:

$$\begin{cases} \dot{\mathbf{x}} = \mathbf{A}\mathbf{x} + \mathbf{B}\mathbf{u} \\ \mathbf{y} = \mathbf{C}\mathbf{x} + \mathbf{D}\mathbf{u}. \end{cases} \quad (1)$$

The system is identified as a passive one if the following criterion is satisfied for all the feasible input vectors  $\mathbf{u}(t)$  and output vectors  $\mathbf{y}(t)$ .

$$\int_0^t \mathbf{u}^T(\tau)\mathbf{y}(\tau)d\tau \geq E(\mathbf{x}(t)) - E(\mathbf{x}(0)) \quad (2)$$

where the left side of (2) is the defined energy flowing into the system,  $\mathbf{x}(t)$  is the system state variable, and  $E(t)$  is the Lyapunov energy function, indicating that the system is passive when the energy injection of the system is not less than the energy stored in the system.

Although (2) is a standard passivity definition, it is still a theoretical criterion that is not explicit enough for practical industry applications. Hence, the following simplified description is introduced.

A linear time-invariant system can be described as (3) in the frequency domain.

$$\begin{aligned} y(s) &= G(s)u(s) \\ G(s) &= C(sI - A)^{-1}B + D \end{aligned} \quad (3)$$

The system in (3) is passive if and only if:

- 1)  $G(s)$  has no poles on the right half plane (RHP).
- 2) The Nyquist plot of  $G(s)$  lies entirely in the closed RHP.

It can be concluded that a passive system is intrinsically stable according to (3) since the system has no closed-loop poles in the RHP. The PBSC has a valuable feature, i.e. the parallel connection of two passive systems is still passive, since the supplied energy is larger than the stored energy in each subsystem. Meanwhile, depending on superposition theory, the total supplied energy is greater than the total stored energy in the parallel system. Hence, paralleling the passive subsystems does not violate the passivity of the overall system. As shown in Fig. 1, multiple subsystems usually coexist in a DC microgrid with the interface converters interconnected in parallel. If all the subsystems in the DC microgrids are passive, the DC microgrids with all these parallel subsystems are passive. Therefore, the stability of the DC microgrids is ensured.

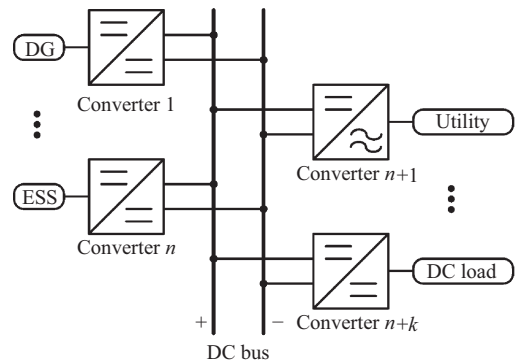


Fig. 1. Typical configuration of DC Microgrids.

## III. MODELING OF PARALLEL CONVERTERS AND PASSIVITY ANALYSIS

### A. A Representative DC Microgrid

The configuration of the DC microgrid under study is depicted in Fig. 2. It is comprised of a distributed generation unit, i.e., a boost converter with a photovoltaic (PV) array, an energy storage system (ESS), i.e., a battery interfaced with a bidirectional buck/boost converter, a CPL, i.e., a resistor interfaced with a buck converter, and a resistive load. The CPL has more severe influence on system stability due to its negative

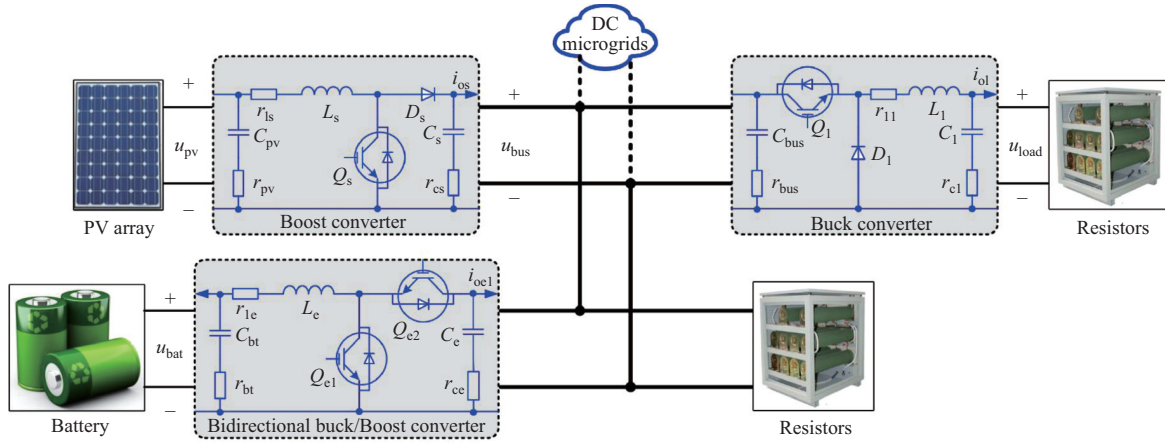


Fig. 2. The proposed topology of DC Microgrids.

incremental impedance, which shows the effectiveness of the proposed passivity design approach.

This typical DC microgrid offers three primary operating modes. In mode I, with sufficient solar irradiation or sudden load increase, the PV converter runs in maximum power point tracking (MPPT) mode and the ESS is in charge of establishing the DC bus voltage. In mode II, with sufficient solar irradiation and low state-of-charge (SoC) of the ESS, the PV converter runs in constant voltage controlled (CVC) mode to establish the DC bus voltage while the ESS is charged to absorb power from the DC bus. In mode III, with insufficient solar irradiation and low SoC of the ESS, the PV module and ESS establish the DC bus simultaneously with droop control as their outer control loops. Here, the PV converter has two operation modes, i.e. MPPT and CVC, where the constant voltage refers to the DC bus voltage. ESS also has two types of operational modes, i.e. charging and discharging modes. In the MPPT mode, the PV converter supplies maximum power to the DC microgrids. In the constant-current charging mode, the ESS absorbs constant power from the DC microgrids. In these two cases, the PV converter and ESS can be regarded as constant power sources and they cannot be used to stabilize the DC bus voltage. The common DC bus voltage in a microgrid can only be guaranteed by using the sources in voltage-controlled mode. This paper focuses on the stability of the DC bus voltage. In mode I, the stability of the DC bus voltage is determined by ESS. In mode II, it is determined by the PV module under CVC control mode. In mode III, it is determined by both the PV sources and ESS. The main power circuits used for PV and ESS are boost converters. Hence, the research in this study focuses on the stabilization methods for boost converters.

### B. Small-signal Modeling of the Proposed System

As described in Section II, the PBSC is an energy-based stability theory and the criterion is implemented on the basis of system input/output transfer functions, which means that the system passivity can be analyzed by using the small-signal model. In order to discuss the impact of the fluctuations of output voltage, output current and voltage reference, and study the stability of the parallel converters regulated by using traditional voltage control methods, the comprehensive

small-signal model of each converter is derived. The detailed model of the converter can be derived by using the state-space averaging model [19] or the equivalent ideal DC transformer model method [20]. As described in Section III-A, only boost converters are analyzed here. The small-signal models, using the ideal DC transformers are shown in Fig. 3.

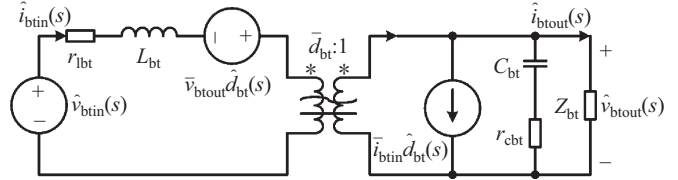


Fig. 3. The small-signal model using the DC transformer of the boost converter.

In Fig. 3, “ $\hat{\cdot}$ ” denotes the small-signal perturbation of each variable, and “ $\bar{\cdot}$ ” denotes the corresponding steady-state variable. The open-loop transfer function of the boost converter can be derived using the small-signal model. The highlighted transfer functions to be studied include the duty-cycle-to-output transfer function  $G_{vd\_bt}(s)$ , the input-to-output transfer function  $G_{vi\_bt}(s)$ , and the converter output impedance  $Z_{btout}(s)$ . According to the voltage and current relationship between the primary and secondary sides of the ideal transformers, the exact definitions of the transfer functions are derived as follows:

$$G_{vd\_bt}(s) = \left. \frac{\hat{v}_{btout}(s)}{\hat{d}_{bt}(s)} \right|_{\hat{v}_{btin}(s)=0} = \frac{Z_{bt}(\bar{v}_{btout}\bar{d}_{bt} - \bar{i}_{btin}r_{lbt} - \bar{i}_{btin}L_{bt}s)(r_{cbt}C_{bt}s + 1)}{L_{bt}C_{bt}(Z_{bt} + r_{cbt})s^2 + [\bar{d}_{bt}^2 Z_{bt}r_{cbt}C_{bt} + L_{bt} + (Z_{bt} + r_{cbt})r_{lbt}C_{bt}]s + (r_{lbt} + \bar{d}_{bt}^2 Z_{bt})} \quad (4)$$

$$G_{vi\_bt}(s) = \left. \frac{\hat{v}_{btout}(s)}{\hat{v}_{btin}(s)} \right|_{\hat{d}_{bt}(s)=0} = \frac{Z_{bt}\bar{d}_{bt}(r_{cbt}C_{bt}s + 1)}{L_{bt}C_{bt}(Z_{bt} + r_{cbt})s^2 + [\bar{d}_{bt}^2 Z_{bt}r_{cbt}C_{bt} + L_{bt} + (Z_{bt} + r_{cbt})r_{lbt}C_{bt}]s + (r_{lbt} + \bar{d}_{bt}^2 Z_{bt})} \quad (5)$$

$$Z_{btout}(s) = \left. \frac{\hat{v}_{btout}(s)}{-\hat{i}_{btout}(s)} \right|_{\substack{\hat{v}_{btin}(s)=0 \\ \hat{d}_{bt}(s)=0}} =$$

$$\frac{Z_{bt}(L_{bt}s + r_{lbt})(r_{cbt}C_{bt}s + 1)}{L_{bt}C_{bt}(Z_{bt} + r_{cbt})s^2 + [d_{bt}^2 Z_{bt} r_{cbt} C_{bt} + L_{bt} + (Z_{bt} + r_{cbt})r_{lbt} C_{bt}]s + (r_{lbt} + d_{bt}^2 Z_{bt})} \quad (6)$$

where  $\bar{v}_{btout}$ ,  $\bar{i}_{btin}$ ,  $\bar{d}_{bt}$  are steady-state values and they can be obtained as:

$$\begin{cases} \bar{d}_{bt} = \bar{v}_{btin}/\bar{v}_{btout} \\ \bar{v}_{btout} = Z_{bt}\bar{v}_{btin}\bar{d}_{bt}/(r_{lbt} + Z_{bt}\bar{d}_{bt}^2) \\ \bar{i}_{btin} = \bar{v}_{btin}/(r_{lbt} + Z_{bt}\bar{d}_{bt}^2). \end{cases} \quad (7)$$

According to (4), (5), and (6) the following mathematical representations of the converters can be concluded:

$$\hat{v}_{btout}(s) = G_{vd\_bt}(s)\hat{d}_{bt}(s) + G_{vi\_bt}(s)\hat{v}_{btin}(s) + Z_{btout}(s)\hat{i}_{btout}(s). \quad (8)$$

According to the open-loop mathematical representation and voltage mode control (VMC) [20], the corresponding closed-loop model is shown in Fig. 4, where  $\hat{v}_{btref}(s)$  represents the perturbation induced by droop control in the reference voltage,  $\hat{v}_{btin}(s)$  represents the perturbation induced by battery voltage fluctuations, and  $\hat{i}_{btout}(s)$  represents the perturbation in the output current. In mode I and mode II, as introduced in Section III-A, the PV module and ESS interfaced via boost converters do not need droop controllers in their control diagram. The corresponding closed-loop model is shown in the internal dotted box with solid lines in Fig. 4, where  $G_{cvt}(s)$  and  $H_{bt}(s)$  are the transfer function of the voltage controller and the sampling network respectively.  $H_{bt}(s)$  can be regarded as '1' here. On the other hand, in mode III, the PV module and the ESS both run in droop-controlled mode to regulate the DC bus voltage. Their closed-loop models are implemented on the basis of the original one used in mode I and mode II with droop control incorporated, i.e.,  $u_{ref} = u_N - k \cdot i_{btout}$ , where  $u_N$  is the converter output voltage at no load and  $k$  is the droop coefficient. Note that the perturbation  $\hat{u}_N$  equals zero in the small-signal model. The corresponding model of mode III is shown in the external dotted box in Fig. 4.

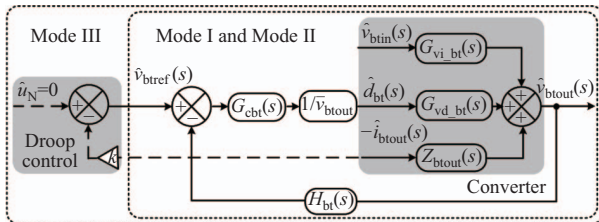


Fig. 4. The closed-loop small-signal representation of the boost converter.

### C. Closed-loop Transfer Function and the Passivity Analysis

Based on the classic control theory, (8) can be rewritten as:

$$\begin{aligned} \hat{v}_{btout}(s) &= \frac{F_{bt}(s)}{1 + F_{bt}(s)}\hat{v}_{btref}(s) + \frac{G_{vi\_bt}(s)}{1 + F_{bt}(s)}\hat{v}_{btin}(s) \\ &\quad - \frac{Z_{btout}(s)}{1 + F_{bt}(s)}\hat{i}_{btout}(s) \\ &= G_{btvrc}(s)\hat{v}_{btref}(s) + G_{btvic}(s)\hat{v}_{btin}(s) \\ &\quad - Z_{btcl}(s)\hat{i}_{btout}(s) \end{aligned} \quad (9)$$

where  $F_{bt}(s) = G_{cvt}(s)G_{vd\_bt}(s)/\bar{v}_{btout}$  and  $F_{bk}(s) = G_{cvt}(s)G_{vd\_bk}(s)/\bar{v}_{bkout}$ .

It can be noted that the closed-loop stability and passivity of converters are influenced by the perturbations of the reference voltage, input voltage and output current. Therefore, the converter passivity can be estimated by using these three transfer functions, i.e.,  $G_{btvrc}(s)$ ,  $G_{btvic}(s)$  and  $Z_{btcl}(s)$ . The PI controller is the most common controller used in DC converters [19]–[21], so the following analysis in this subsection is conducted based on the PI control diagram.

It is worth noting that the denominators of  $G_{btvrc}(s)$ ,  $G_{btvic}(s)$  and  $Z_{btcl}(s)$  for the boost converter are the same. Hence, the poles of these transfer functions can be synthesized in Fig. 5. As shown in Fig. 5, the poles at the real axis move towards the left side and the conjugate complex poles move towards the right side when  $K_I$  increases and  $K_P$  remains constant; and in the meantime, the poles at the real axis move towards the right side and the conjugate complex poles move towards the left side when  $K_P$  increases and  $K_I$  remains constant. Moreover, the dominant poles are not located in the RHP, which means the closed-loop control diagram is stable with these parameters. However, the PI control can only stabilize itself. While a converter with conventional control is connected into a stable system, the system may become unstable. In contrast, once a passive module with dissipative terminal characteristic is incorporated into a passive system, the whole system is passive and stable. In this case, without considering the internal structure and parameters, the terminal characteristics can ensure the stability of the new system.

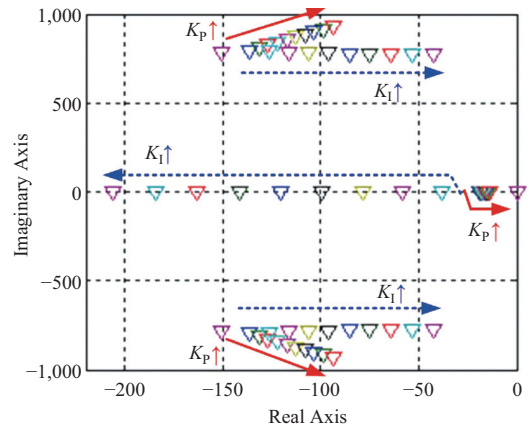


Fig. 5. Location of the dominant poles of the closed-loop transfer functions for boost converters.

In order to conduct the passivity analysis of  $G_{btvrc}(s)$ ,  $G_{btvic}(s)$  and  $Z_{btcl}(s)$ , it is necessary to discuss the Nyquist plots of these transfer functions. As described in Section II, if their Nyquist plots lie entirely within the closed RHP, the converters are passive. Fig. 6 shows the Nyquist plot of  $G_{btvrc}(s)$ ,  $G_{btvic}(s)$  and  $Z_{btcl}(s)$ . In Fig. 6, it can be seen that all the Nyquist plots of the boost converter move outwards when  $K_P$  or  $K_I$  increases. While they always have partial plots located in the left half plane, which means manipulating the parameters of the PI controller cannot ensure the passivity of the boost converter.

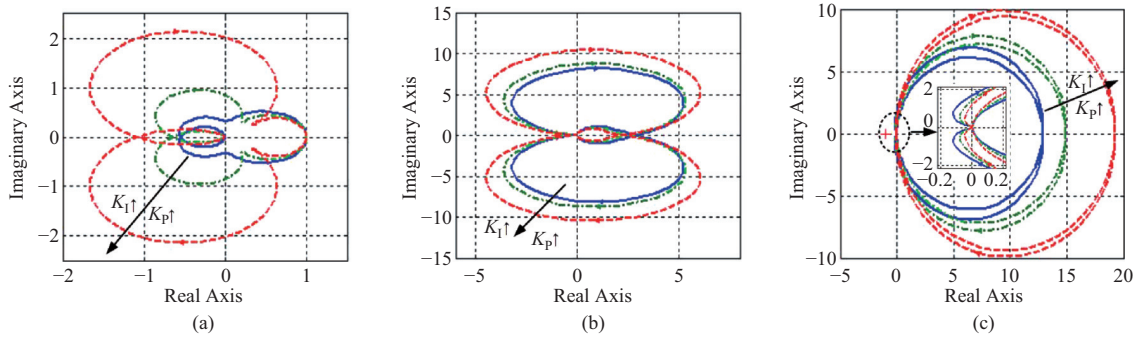


Fig. 6. The Nyquist plots of (a)  $G_{btvrcl}(s)$ , (b)  $G_{btviel}(s)$  and (c)  $Z_{btcl}(s)$ .

#### IV. IMPROVED CONTROL STRATEGY

##### A. Improved Closed-loop Transfer Function

The closed-loop transfer function is improved to design a converter control diagram complying with the PBSC described above. Many converters in DC microgrids adopt the voltage feed-forward loop to offer extra positive admittance and thereby enhance the stability [19]. However, the design process of the feed-forward controller is very complicated and this method only considers the output impedance passivity.

Although  $G_{btvrcl}(s)$  and  $G_{btviel}(s)$  are not passive, adding a derivative term in the corresponding closed-loop transfer functions can improve their passivity [18]. Hence, a combined control diagram with a PI controller and HPF is suggested to replace the conventional PI controller, which will ensure the passivity of  $G_{btvrcl}(s)$  and  $G_{btviel}(s)$ . Then, the current feedback loop is added to the output side of the PI and HPF, which will ensure the passivity of  $Z_{btcl}(s)$  together with the combination of the PI controller and HPF. The improved control strategy is marked in red lines, as shown in Fig. 7. The transfer function  $G_{pidt}(s)$  can be described as  $K_P + K_I/s + K_D s/(\tau_d s + 1)$ . In order to ensure the control bandwidth,  $\tau_d$  is suggested to be  $T_s$ , which represents the control period of the converter.

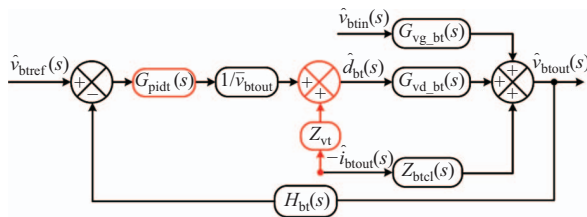


Fig. 7. The improved closed-loop control diagram of the boost converter.

According to Fig. 7 and the classic control theory [22], (9) can be modified as follows:

$$\begin{aligned} \hat{v}_{btout}(s) &= \frac{F'_{bt}(s)}{1 + F'_{bt}(s)} \hat{v}_{btref}(s) + \frac{G_{vi\_bt}(s)}{1 + F'_{bt}(s)} \hat{v}_{btin}(s) \\ &\quad - \frac{Z_{vt} G_{vd\_bt}(s) + Z_{btout}(s)}{1 + F'_{bt}(s)} \hat{i}_{btout}(s) \\ &= G'_{btvrcl}(s) \hat{v}_{btref}(s) + G'_{btviel}(s) \hat{v}_{btin}(s) \\ &\quad - Z'_{btcl}(s) \hat{i}_{btout}(s) \end{aligned} \quad (10)$$

where  $F'_{bt}(s) = G_{pidt}(s)G_{vd\_bt}(s)/\hat{v}_{btout}$ .

##### B. Passivity Analysis

The poles of each input-to-output transfer functions in (10) are different from (9) due to the deployment of the combined PI and HPF control diagram. Meanwhile, the denominators of different terms in (10) are the same. The dominant poles of  $G'_{btvrcl}(s)$ ,  $G'_{btviel}(s)$  and  $Z'_{btcl}(s)$  for boost converters with a different  $K_D$  are shown in Fig. 8.

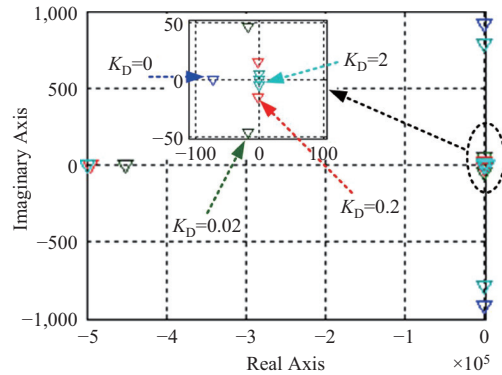


Fig. 8. Location of the dominant poles of the modified closed-loop transfer functions.

In Fig. 8, real poles move away from the original point and the complex poles are close to the original point when the deviation factor  $K_D$  increases from 0. The complex poles denote that the system has a damped oscillating response. However, all of the zeroes still locate in the left half plane (LHP), which means the closed-loop is stable.

In order to analyze the passivity of the boost converter considering the three modified input channels, the plots with different  $K_D$  values are shown in Fig. 9, where  $Z_{vt} = 0.5$ . All Nyquist plots move entirely to the RHP with  $K_D$  increasing from 0 to 2, and the converters become passive. It can be derived that  $G'_{btvrcl}(s)$  and  $G'_{btviel}(s)$  are not influenced by  $Z_{vt}$ . The influence on  $Z'_{btcl}(s)$  is shown in Fig. 10, where different values of  $Z_{vt}$  are considered and  $K_D$  is set to 0.02. The Nyquist plots move entirely to the RHP when  $Z_{vt}$  increases. However, the Nyquist plots of the boost converter are partially within the LHP when  $Z_{vt}$  equals 0 or 0.05, indicating that  $Z_{vt}$  cannot be too large to maintain the passivity.

#### V. SIMULATION VALIDATION

A simulation model with three converters is implemented in MATLAB/Simulink to confirm the proposed control strategy

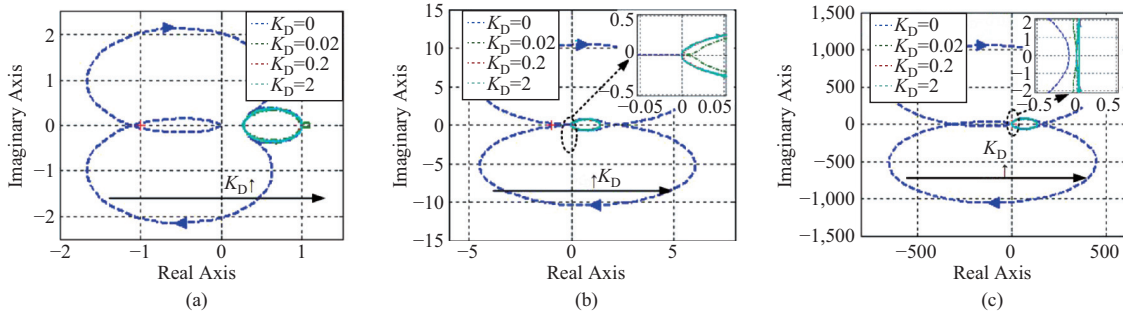


Fig. 9. The Nyquist plots of the modified (a)  $G'_{btvrcl}(s)$ , (b)  $G'_{btvcl}(s)$  and (c)  $Z'_{btcl}(s)$ .

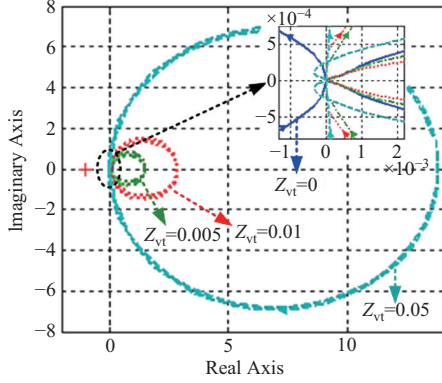


Fig. 10. The Nyquist plots of the modified  $Z'_{btcl}(s)$  with different  $Z_{vt}$ .

based on PBSC. It includes three cases. For Case I, by using the improved passivity-based method in boost converters, the stability operation in mode I and mode II can be guaranteed. For Case II, under the same condition, the potential stability induced by parallel converters can be avoided. In Case III, the DC bus voltage stability can be ensured with the perturbations in reference voltage, input voltage and output current. The system parameters are listed in Table I.

TABLE I  
CONVERTERS CONFIGURATIONS

Type	Parameter	Value
PV converter	$C_{pv}$ ( $\mu\text{F}$ )	100
	$r_{pv}$ ( $\Omega$ )	1e-3
	$L_s$ (mH)	1
	$r_{ls}$ ( $\Omega$ )	5e-2
	$C_s$ ( $\mu\text{F}$ )	400
	$r_{cs}$ ( $\Omega$ )	4e-3
Load converter	$C_{bus}$ ( $\mu\text{F}$ )	200
	$r_{bus}$ ( $\Omega$ )	2e-3
	$L_l$ (mH)	2
	$r_{ll}$ ( $\Omega$ )	8e-2
	$C_l$ ( $\mu\text{F}$ )	200
	$r_{cl}$ ( $\Omega$ )	2e-3
Battery converter	$C_{bt}$ ( $\mu\text{F}$ )	150
	$r_{bt}$ ( $\Omega$ )	1e-3
	$L_e$ (mH)	1.5
	$r_{le}$ ( $\Omega$ )	6e-2
	$C_e$ ( $\mu\text{F}$ )	300
	$r_{ce}$ ( $\Omega$ )	3e-3

#### A. Microgrid Operation in Mode I and Mode II

In mode I, the PV converter operates in MPPT mode, and the ESS converter acts as a source to regulate the bus voltage ( $u_{bus}$ ). In this operational mode, the PV converter

can be controlled as a constant power source and the load with constant power is also connected to the common DC bus. Meanwhile, the ESS operates as a voltage source. The passivity of the microgrid is guaranteed by ensuring the passivity of the ESS converter control system. In mode II, the PV source converter regulates the bus voltage, and the ESS converter operates as a constant power load. In this operational mode, only the PV module operates in voltage-source mode. The passivity of the microgrid is ensured by the passive control of the PV converter. To compare the results of the traditional and the proposed methods, simulation results of the bus voltage with two control strategies are presented for mode I and mode II, as shown in Fig. 11.

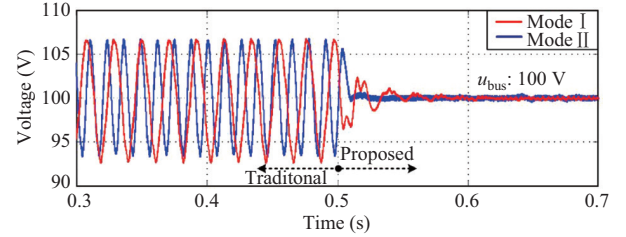


Fig. 11. Simulation results of the bus voltage with controller change in mode I and mode II.

In mode I and mode II, the control methods change from the traditional one to the proposed one at 0.5 s. The voltage oscillations occur under traditional control for the dynamic interaction between the connected converters. The proposed method can effectively damp the voltage oscillation because the passivity of the system is ensured.

For mode I and mode II, the waveforms of  $u_{bus}$  and the output power of each converter under the proposed control strategy are respectively shown in Fig. 12.

The load resistance decreases from 20  $\Omega$  to 10  $\Omega$  at 0.4 s and increases back to 20  $\Omega$  at 0.6 s. It can be seen from Fig. 12(a) and Fig. 12(b) that  $u_{bus}$  is maintained at 100 V in mode I. The load power  $P_{load}$  is approximately equal to the sum of the discharging power  $P_{bat}$  and the PV source power  $P_{pv}$  in the steady state, which indicates the load is powered by the PV source with maximum power and ESS. In Fig. 12(c) and Fig. 12(d),  $u_{bus}$  is also stabilized at 100 V. The PV source power  $P_{pv}$  is approximately equal to the sum of the charging power of  $P_{bat}$  and the load power  $P_{load}$  in the steady state, which means that the PV module is used to establish the DC bus voltage and provide the charging power of the ESS and

the load. The results above prove that the proposed control strategy can ensure the stability of DC microgrids with load step-change in the two operational modes.

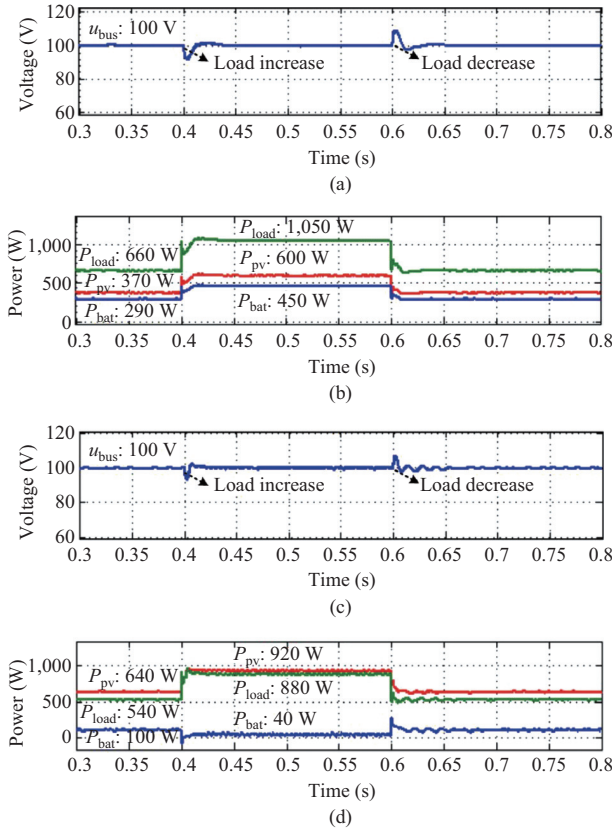


Fig. 12. Simulation results in mode I and mode II. (a) Voltage waveform in mode I. (b) Power waveforms in mode I. (c) Voltage waveform in mode II. (d) Power waveform in mode II.

### B. Microgrid Operation in Mode III

DC microgrids with traditional control methods suffer from degraded stability due to the interactions among converters, while the proposed control strategy can ensure the passivity of the DC microgrids with parallel-connected converters and thereby ensure the system stability. In mode III, the DC bus voltage is controlled by using the PV converter and the ESS converter simultaneously. By using the passivity-based control approach, when the passivity of each converter is achieved, the passivity of the DC microgrid with parallel passive modules can be ensured. In order to verify this point, Nyquist plots of the PV converter, ESS converter and the system are applied in Fig.13. All Nyquist plots lie entirely in the closed RHP which implies the passivity of the DC microgrid.

Accordingly, the operational simulations with traditional and proposed control strategies are conducted for mode III. The comparative simulation results are shown in Fig. 14.

The control strategy changes from the traditional method to the proposed strategy at 0.4 s. It can be seen from Fig. 14 that before activating the proposed passivity-based control scheme, oscillations can be found in the waveforms of  $u_{bus}$  and the output power of each converter, so the system is not asymptotically stable. At 0.4 s, when the proposed method is

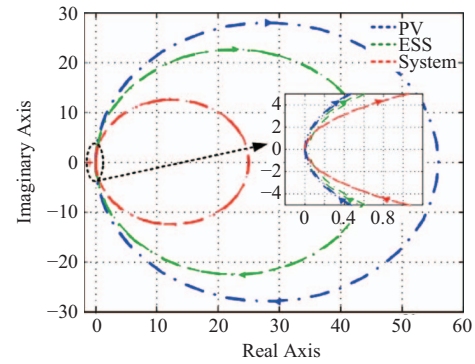


Fig. 13. The Nyquist plots of the PV converter, ESS converter and the DC microgrid.

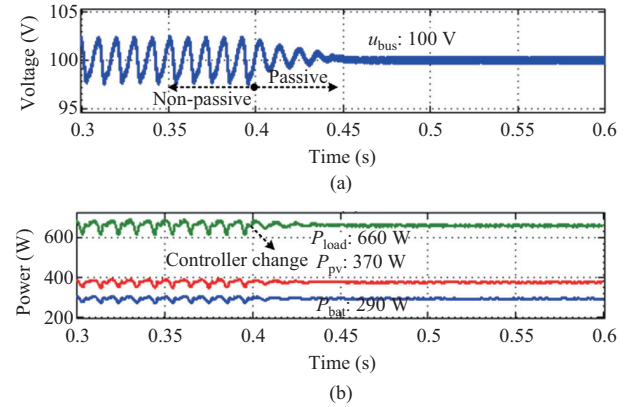


Fig. 14. Simulation results with the controller change in mode III. (a) Voltage waveform. (b) Power waveform.

activated, the oscillations in the waveforms of  $u_{bus}$  and the output power of each converter are minimized. Mode III can be regarded as the combination of mode I and mode II with the consideration of parallel converters. The effectiveness of the proposed method in mode III verifies the applicability of the passivity-based method, which thereby tackles the obstacles of the degraded stability in microgrids with parallel converters.

### C. Stability Analysis under the Proposed Control Method with Three Types of Perturbations in Mode III

It should be noted that the perturbations here refer to the disturbances involved in different channels, i.e. load variation, input voltage, and reference voltage used in droop control. In mode III, these three types of perturbations coexist while in the other operation modes, it is unnecessary to consider the perturbations in the reference voltage since droop control is not employed. For brevity, the most complicated operational mode, i.e. mode III, is taken as an example here to test the impacts of different types of perturbations.

For the stability analysis with output current perturbations, as the output current is primarily influenced by load variations, simulations with load step-change are performed to test the impact of the output current perturbation on the DC bus voltage stability. The simulation results are shown in Fig. 15.

The load resistance decreases from 20  $\Omega$  to 10  $\Omega$  at 0.4 s and increases back to 20  $\Omega$  at 0.6 s. It can be seen from Fig. 15 that  $u_{bus}$  decreases with the decrease of load, at

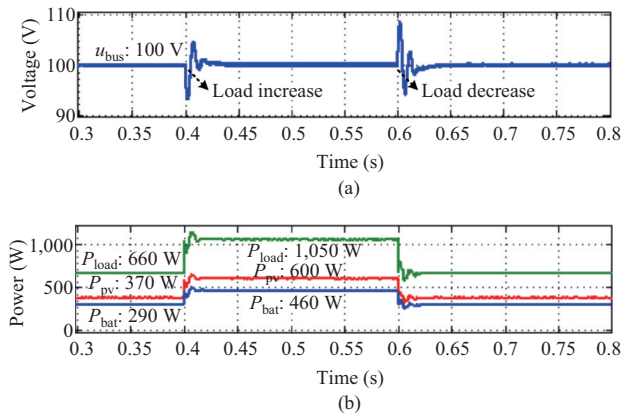


Fig. 15. Simulation results with load step-change. (a) Voltage waveform. (b) Power waveform.

this time the PV and ESS converter increase their output power to maintain the bus voltage at 100 V, and vice versa. The load power is approximately equal to the sum of the discharging power  $P_{bat}$  and the PV source power  $P_{pv}$  in the steady state. The results above prove that the proposed control strategy can ensure the stability of the DC microgrids under output current perturbation. For the stability analysis with input voltage perturbations, the simulation results with input voltage step-change are shown in Fig. 16.

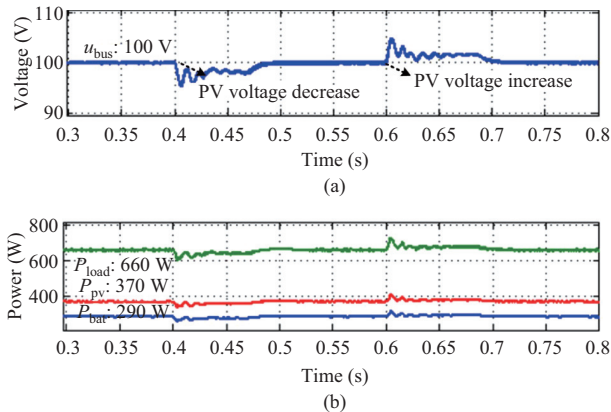


Fig. 16. Simulation results with input voltage step-change. (a) Voltage waveform. (b) Power waveform.

As shown in Fig. 16, the PV input voltage decreases from 100 V to 90 V at 0.4 s and increases back to 100 V at 0.6 s. It can be seen from Fig. 4 and (9) that the DC bus voltage is influenced by the input voltage. As shown in Fig. 16, when the input voltage drops, the output voltage is reduced accordingly, and vice versa. In mode III, the DC bus voltage is regulated by using two parallel converters, so there is a transient process for adjusting the DC bus voltage back to its reference value. The output power of each converter also changes along with the input PV voltage. By using the passivity-based control method, the impact of perturbations can be avoided and the output power of each converter can finally return to its original value. The above results prove that the proposed control strategy can ensure the stability of the DC microgrids with the perturbations in the input voltage.

For stability analysis with reference voltage perturbations, the simulation tests are conducted below. The reference perturbation cannot be ignored when droop control is adopted for multiple converters when they all regulate DC bus voltage simultaneously. Simulation results with reference voltage perturbation are shown in Fig. 17.

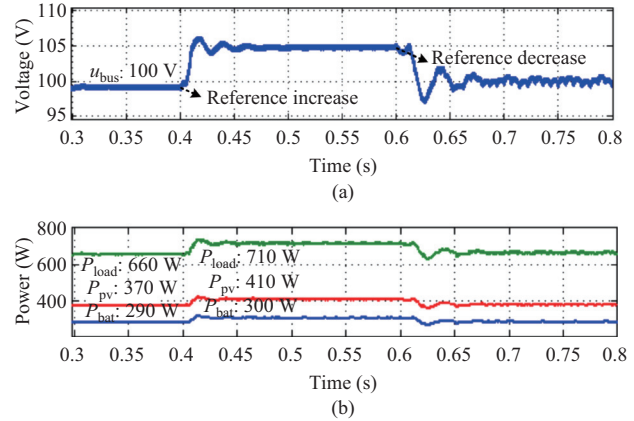


Fig. 17. Simulation results with reference voltage perturbation in storage-dominating mode. (a) Voltage waveform. (b) Output power waveform.

The perturbation in the battery output reference voltage is assumed to increase from 100 V to 105 V at 0.4 s and decrease back to 100 V at 0.6 s. It is obvious that  $u_{bus}$  follows the reference voltage and changes from 100 V to 105 V after 0.4 s and then goes back to 100 V after 0.6 s, as shown in Fig. 17. The load power  $P_{load}$  is approximately equal to the sum of the discharging power  $P_{bat}$  and the PV source power  $P_{pv}$  in steady state. The above results prove that the proposed control strategy can ensure the stability of droop-controlled DC microgrids with reference voltage perturbations.

#### D. Transition between Different Mode

To further evaluate the practicability of the proposed control strategy, for the case of operational mode transition, the system dynamic performance is simulated. For simplification, the mode transition cases between mode II and mode III are implemented in Fig. 18. The waveforms of  $u_{bus}$  and the output power for each converter under the proposed control strategy are respectively shown in Fig. 18.

The operational mode changes from mode III to mode II at 0.5 s, and goes back to mode III at 0.7 s. Accordingly, the battery status is changed from CVC mode to the charging mode at 0.5 s, and goes back to CVC mode at 0.7 s. It is obvious that the proposed control method could stabilize  $u_{bus}$  and achieve the expected values of output power for each converter under mode transition.

## VI. CONCLUSION

The PBSC has been applied to DC microgrids; however, only the output impedance passivity is commonly considered for each converter, which cannot ensure the overall bus voltage stability of the DC microgrids. In the small-signal model of the DC microgrids, the perturbations of the input voltage, output current and reference voltage of the converters have



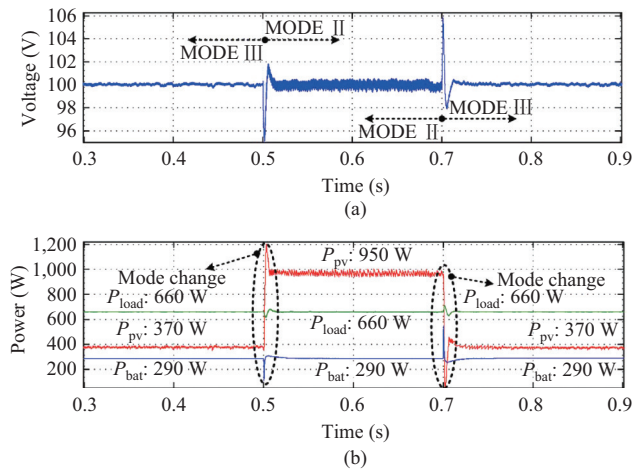


Fig. 18. Simulation results of mode transition between mode II and mode III. (a) Voltage waveform. (b) Output power waveform.

inevitable impacts on the DC bus voltage stability, which means that if and only if all these three passivity requirements are satisfied, will the parallel converter system be passive and stable. An improved active stabilization strategy of the interface converters in DC microgrids is proposed. In particular, a combined control diagram with a PI controller and a first-order HPF is employed in the proposed stabilization algorithm to satisfy the passivity of the input voltage and reference voltage with respect to output voltage. Meanwhile, an output current feedback control loop is introduced to ensure the output impedance passivity. The proposed control method guarantees the overall passivity of the control diagram considering the perturbations from the input channels of the input voltage, reference voltage and output impedance.

## REFERENCES

- [1] T. Dragičević, X. N. Lu, J. C. Vasquez, and J. M. Guerrero, "DC microgrids—Part I: A review of control strategies and stabilization techniques," *IEEE Transactions on Power Electronics*, vol. 31, no. 7, pp. 4876–4891, Jul. 2016.
- [2] T. Dragičević, X. N. Lu, J. C. Vasquez, and J. M. Guerrero, "DC microgrids—Part II: A review of power architectures, applications, and standardization issues," *IEEE Transactions on Power Electronics*, vol. 31, no. 5, pp. 3528–3549, Jul. 2016.
- [3] A. Kwasinski and C. N. Onwuchekwa, "Dynamic behavior and stabilization of DC microgrids with instantaneous constant-power loads," *IEEE Transactions on Power Electronics*, vol. 26, no. 3, pp. 822–834, Mar. 2011.
- [4] H. Kakigano, Y. Miura, and T. Ise, "Low-voltage bipolar-type DC microgrid for super high quality distribution," *IEEE Transactions on Power Electronics*, vol. 25, no. 12, pp. 3066–3075, Dec. 2010.
- [5] K. Strunz, E. Abbasi, and D. N. Huu, "DC microgrid for wind and solar power integration," *IEEE Journal of Emerging and Selected Topics in Power Electronics*, vol. 2, no. 1, pp. 115–126, Mar. 2014.
- [6] H. Kakigano, M. Nomura, and T. Ise, "Loss evaluation of DC distribution for residential houses compared with AC system," in *Proceedings of IPEC, Sapporo, Japan, 2010*, pp. 480–486.
- [7] A. Pratt, P. Kumar, and T. V. Aldridge, "Evaluation of 400V DC distribution in Telco and data centers to improve energy efficiency," in *Proceedings of the 29th International Telecommunications Energy Conference, Rome, Italy, 2007*, pp. 32–39.
- [8] R. D. Middlebrook, "Input filter considerations in design and application of switching regulators," in *Proceedings of IEEE Industry Applications Society Annual Meeting, 1976*, pp. 366–382.

- [9] C. M. Wildrick, F. C. Lee, B. H. Cho, and B. Choi, "A method of defining the load impedance specification for a stable distributed power system," *IEEE Transactions on Power Electronics*, vol. 10, no. 3, pp. 280–285, May 1995.
- [10] X. G. Feng, Z. H. Ye, K. Xing, F. C. Lee, and D. Borojovic, "Impedance specification and impedance improvement for dc distributed power system," in *Proceedings of the 30th IEEE Power Electronics Specialists Conference, 1999*, vol. 2, pp. 889–894.
- [11] S. D. Sudhoff, S. F. Glover, P. T. Lamm, D. H. Schmucker, and D. E. Delisle, "Admittance space stability analysis of power electronic systems," *IEEE Transactions on Aerospace and Electronic Systems*, vol. 36, no. 3, pp. 965–973, Jul. 2000.
- [12] S. D. Sudhoff and S. F. Glover, "Three-dimensional stability analysis of dc power electronics based systems," in *Proceedings of the 31st Annual Power Electronics Specialists Conference, 2000*, vol. 1, pp. 101–106.
- [13] A. Riccobono and E. Santi, "Comprehensive review of stability criteria for DC power distribution systems," *IEEE Transactions on Industry Applications*, vol. 50, no. 5, pp. 3525–3535, Sep./Oct. 2014.
- [14] J. E. Colgate, "The control of dynamically interacting system," Ph. D. dissertation, Massachusetts Institute of Technology, Cambridge, 1988.
- [15] A. Riccobono and E. Santi, "Stability analysis and design of stable dc distribution systems through positive feed-forward control using a novel passivity-based stability criterion," in *Proceedings of the 28th Annual IEEE Applied Power Electronics Conference and Exposition, 2013*, pp. 1693–1701.
- [16] Y. J. Gu, W. H. Li, and X. N. He, "Passivity-based control of DC microgrid for self-disciplined stabilization," *IEEE Transactions on Power Systems*, vol. 30, no. 5, pp. 2623–2632, Sep. 2015.
- [17] J. C. Willems, "Dissipative dynamical systems Part I: General theory," *Archive for Rational Mechanics and Analysis*, vol. 45, no. 5, pp. 321–351, Jan. 1972.
- [18] J. C. Willems, "Dissipative dynamical systems Part II: Linear systems with quadratic supply rates," *Archive for Rational Mechanics and Analysis*, vol. 45, no. 5, pp. 352–393, Jan. 1972.
- [19] X. N. Lu, K. Sun, J. M. Guerrero, J. C. Vasquez, L. P. Huang, and J. H. Wang, "Stability enhancement based on virtual impedance for DC microgrids with constant power loads," *IEEE Transactions on Smart Grid*, vol. 6, no. 6, pp. 2770–2783, Nov. 2015.
- [20] R. W. Erickson, *Fundamentals of Power Electronics*, 2nd ed., Kluwer Academic, Norwell, MA, USA, 2001.
- [21] M. Cupelli, L. Zhu, and A. Monti, "Why ideal constant power loads are not the worst case condition from a control standpoint," *IEEE Transactions on Smart Grid*, vol. 6, no. 6, pp. 2596–2606, Nov. 2015.
- [22] W. K. Chen, *Linear Networks and Systems*, Wadsworth, Belmont, CA, 1993, pp. 123–135.



**Jiaqi Yu** received the B.S. degree in electrical engineering from North University of China, Taiyuan, China, in 2007. She is currently pursuing the Ph.D. degree in Hunan University, Changsha, China. Her current research interests include power quality, distributed generation and micro-grid.



**Jingrong Yu** received the B.S. and Ph.D. degrees from Hunan University, Changsha, China, in 2004 and 2009, respectively. She is currently an Associate Professor in the School of Information Science and Engineering, Central South University, Changsha, China. Her current research interests include power quality, renewable energy systems, distributed generation, multilevel converters and DC micro-grid.



**Yue Wang** received the B.S. degree in electrical engineering from Central South University, Changsha, China, in 2015, where she is currently pursuing the M.S. degree in electrical engineering. Her current research interests include renewable energy systems, distributed generation, and DC micro-grid.

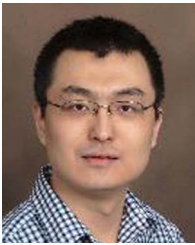


**Dongbo Zhao** (M'14–SM'16) received his B.S. degree from Tsinghua University, China in 2008, M.S. degree from Texas A&M University, College Station, Texas in 2010, and Ph.D. degree from Georgia Institute of Technology, Atlanta, Georgia in 2015, all in electrical engineering. Since 2014 he is the Lead Engineer at Eaton Corporation in the corporate research and technology department. He has worked with ABB Inc. US Corporate Research Center located in Raleigh, NC from 2010 to 2011.

His research interests include power system control, protection, reliability analysis, transmission and distribution automation, and electric market optimization.



**Yijia Cao** (M'98–SM'13) received the B.S. degree in mathematics from Xi'an Jiaotong University, Xi'an, China, in 1988, the M.S. degree in computer science and the Ph.D. degree in electrical engineering from Huazhong University of Science and Technology (HUST), Wuhan, China, in 1991 and 1994, respectively. Since 2008, he has been a Full Professor and Vice President of Hunan University, Changsha, China. His research interests include power system stability control and the application of intelligent systems in power systems.



**Xiaonan Lu** (M'14) received the B.E. and Ph.D. degrees in electrical engineering from Tsinghua University, Beijing, China, in 2008 and 2013, respectively. In Jan. 2015, he joined the Energy Systems Division, Argonne National Laboratory, where he is currently a postdoc appointee. His research interests include modeling and control of power electronic converters in renewable energy systems and microgrids, hardware-in-the-loop real-time simulation, distribution automation, etc. Dr. Lu received the Outstanding Reviewer Award for *IEEE Transactions*

on *Power Electronics* in 2013 and the Outstanding Reviewer Award for *IEEE Transactions on Smart Grid* in 2015.

© 2018. Notwithstanding the ProQuest Terms and Conditions, you may use this content in accordance with the associated terms available at <https://ieeexplore.ieee.org/Xplorehelp/#/accessing-content/open-access>.